



Performance Study of Buried Pipelines under Static Loads

Mahdi J. Alanazi¹, Yang Qinghua^{1*}, Khalil Al-Bukhaiti^{1*}

¹ Southwest Jiaotong University, Chengdu, Sichuan, China.

Received 10 October 2021; Revised 01 December 2021; Accepted 16 December 2021; Published 01 January 2022

Abstract

The possibility of servicing lifelines such as highways, railways, pipelines, and tunnels is of great social importance. The characteristic that separates the buried pipeline from other structures is that its dimensions are very long compared to its other dimensions. Ground vibrations caused by earthquakes, construction activities, traffic, explosions, and machinery can damage these structures. Lifeline integrity can be compromised in two ways: (1) direct damage due to excessive dynamic loading of the lifeline, and (2) indirect damage due to soil failures such as liquefaction, slope instability, and differential settlements. 3D printing (also known as additive manufacturing) is an advanced manufacturing process that can automatically produce complex geometric shapes from a 3D computer-aided design model without tools, molds, or fixtures. This automated manufacturing process has been applied in diverse industries today because it can revolutionize the construction industry with expected benefits. This research study on the performance of buried pipelines under static loads to the structure's safety against the possible development of progressive failure. This research study includes a numerical study, where it was studied many parameters to value the performance of the pipeline. The parameters are (a) the material of the pipeline (steel, traditional concrete, and 3D concrete printed), (b) the thickness of the pipeline (20, 30, and 40 mm), and (c) soil type (moist sandy soil, saturated sandy soil, moist cohesive soil, and saturated cohesive soil). Different results were obtained depending on the type of soil where all pipelines materials' behavior was similar in the case of moist soil.

Keywords: 3D Printed Concrete; Pipeline; Moist Soil; Saturated Soil.

1. Introduction

It is known that the structures located on the surface of the ground are subject to more significant seismic damage than the structures located underground. Where the earthquakes destroyed a lot of buried pipelines [1]; thus, the damage or disruption of the buried gas and water pipelines due to the earthquake leads to economic losses and disruption of lifeline networks.

In recent years, the development of high-strength and ductile composite materials in earthquake-prone areas has become an important topic for researchers. These materials have many advantages (e.g., experienced high strength and displacement capacity under compression and tension loadings). One of the most common composite materials is Textile-Reinforced Concrete (TRC), which includes a fine-grained concrete matrix and high-strength textile fabric reinforcement made of alkali-resistant glass fibers or polyvinyl alcohol (PVA) fibers. TRC can be used as structural strengthening material such as Fiber Reinforced Polymer (FRP); also, it can be used as a structural element [2]. Viparelli et al. studied pre-stressed concrete large-diameter pipes joint behavior during earthquakes [3]. Susan et al.

* Corresponding author: qhyang@swjtu.edu.cn; khalil2020@my.swjtu.edu.cn

<http://dx.doi.org/10.28991/CEJ-2022-08-01-01>



© 2022 by the authors. Licensee C.E.J, Tehran, Iran. This article is an open access article distributed under the terms and conditions of the Creative Commons Attribution (CC-BY) license (<http://creativecommons.org/licenses/by/4.0/>).

studied the reinforced concrete pipeline crack retrofitted with the Fibre Reinforced Polymer (FRP) [4]. Roudsari et al. were evaluated the failure criterion of Glass Reinforced Polymer (GRP) pipes [5]. Ozdemir et al. have reported the risk of damage to a high-pressure steel natural gas pipeline and a concrete sewer pipe due to the operation of a pavement breaker utilizing the 2.5D coupled Finite Element-Boundary Element (FE-BE) methodology [6, 7]. Trautmann et al. were mentioned the soil-pipelines interaction related to the weight of the soil above the pipelines [8, 9], Sakanoue and Yoshizaki were reported that lightweight backfill is effective for the enhancement of earthquake resistance of buried pipelines [10].

Additive manufacturing (also known as three-dimensional (3D) printing) is an advanced manufacturing process that can automatically produce complex geometric shapes from a 3D computer-aided design model without any tools, molds, or fixtures. This automated manufacturing process has been applied in many areas of diverse industries today as it has the potential to revolutionize the construction industry [11–14]; this technology has many advantages (e.g., improving structural capacity, decreasing the cost of the project by decreasing material consumption and waste, fast in design and production, strong and lightweight parts, environmentally friendly, and improved accuracy and site safety [15–21]). On the other hand, this technology has many disadvantages and challenges. (e.g., its need engineers with digital experience and a new method of considering for the design and verification of structures) [22–24].

Concrete is considered a quasi-brittle material that is weak in tension but strong in compression [25]. Generally, concrete with reinforcement steel bars has more tensile, shear, and flexural capacity than traditional concrete. Therefore, 3D Concrete Printing (3DCP) structural elements have to be reinforced to increase their performance. Thus, 3DCP required new techniques to improve the ductility so that it can be used in areas subject to strong lateral loads such as earthquakes [26–28]. Installing reinforcement in 3DCP is complicated because the printing process requires enough space above the layer being extruded to allow for the movement of the nozzle [29]. This issue can be overcome by either installing reinforcement after or before the printing or using the reinforcing cable, mesh, and fiber during concrete extrusion or printing the reinforcement simultaneously [29–34]. Also, it can reduce the required reinforcement by using post-tensioning techniques, which reduces the required tensile strength of the 3DCP structure [29].

Numerical analysis has many advantages over experimental testing (e.g., it is a less expensive way to get the results than testing many specimens). In addition, using numerical simulation can study a lot of parameters that affect the behavior of the structure. 3D Reinforced Concrete Printed modeling is important to consider its effect on the general behavior of the structure, thus designing the structural elements correctly. On the other hand, incorrect modeling has negative effects because it gives a misconception about the behavior of the structure.

The pipe-soil interaction along with the pipe parts is the most parameter that affects the buried pipeline's static and dynamic structural performance. To control the performance of the buried pipelines, there are a lot of critical factors, such as soil cohesion, density, and friction angle (soil shear strength properties). Generally, these parameters are commonly considered independently, but in the case of natural soil, these parameters significantly influence the performance of the buried pipe.

This research study on the performance of buried pipelines under static load to the structure's safety against the possible development of progressive failure. This research study includes a numerical study, where it was studied many parameters to value the performance of the pipeline. The parameters are the material of the pipeline, the thickness of the pipeline, and soil type. Different results were obtained depending on the type of soil. The paper continues with Finite Element Analysis (FEM), including Constitutive Material Models and Interaction models. Next, the Parameters study. Then, Results and discussion. Finally, conclusions have been drawn suggesting the possible application directions for the performance study of buried pipelines under static loads.

2. Finite Element Analysis (FEM)

In this study, the pipeline was considered used for the water supply lifeline. The DN 1500 pipeline outer diameter was 1524 mm with different thicknesses (t), the length of the pipeline (L) was 100 m [35, 36]. Figure 1 shows the dimension of the DN 1500 pipeline

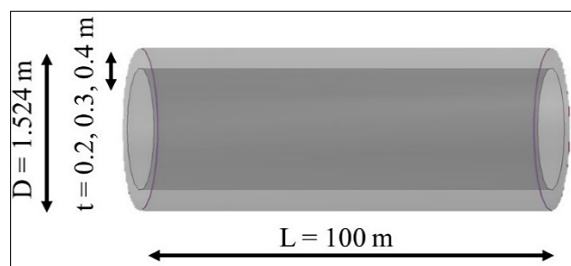


Figure 1. Dimensions of the pipeline model

The soil was considered as a cube shape with a buried pipeline on one centerline. The length of the soil (L) was 100 m. The width (W) and height (H) of soil were 10, 5 m, respectively. To ensure the affordable space in which the pipeline with soil is failed when finite element analysis is used. The buried depth of pipeline from the pipe's crown (h) was 6 m from the top surface of the soil to the crest of the pipeline, as shown in Figure 2.

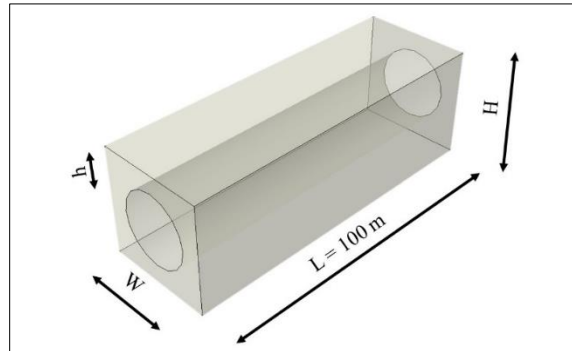


Figure 2. Dimensions of the soil model [36]

In this study, ABAQUS 2020 software was used to simulate the general behavior of buried pipelines due to a finite element analysis of buried pipeline static loads. To analyze a buried pipeline, it is necessary to accept three basic assumptions as follows.

- The welding between parts of pipelines is ignored.
- Elastomeric soils featuring Mohr-Coulomb theory and pipeline are isotropic, elastic, and ideally plastic.
- The perfect interaction between the pipeline and the soil without defects.

There are some limitations; it is difficult to know the real performance of pipelines by not considering weld points between pipeline parts, applying the fully bonded contact area between pipeline and soil, and adapting the simplified material properties of both soil and pipelines. This is because the above three assumptions are not related to the real performance of the pipeline. However, these assumptions make the analysis easier because typical pipeline performance can be studied by ignoring small, irreversible effects on pipeline performance.

2.1. Constitutive Material Models

A three-dimensional 8-node linear brick, reduced integration, hourglass control (C3D8R) were used to model concrete pipeline, 3D printed concrete pipeline, and soil. In the global directions, that element has three freedom translational degrees for every node. This element can lead to modeling any complex geometry and performing nonlinear analyses, including contact, plasticity, and huge deformations. A 4-node doubly curved thin or thick shell, reduced integration, hourglass control, finite membrane strains (S4R) was used to model steel pipeline. Reduced integration was used in the analysis; to decrease the computation time in the special cases of large-scale problems. A disadvantage of using the reduced integration is that it will affect the element stiffness matrix.

• Steel Pipeline

The behavior of steel material used for the pipeline was perfect by an elastic-plastic material response. According to Figure 3. The total deformation (ϵ) elastic deformation (ϵ^{el}), and plastic deformation (ϵ^{pl}) Equation 1 expresses the behavior of steel material.

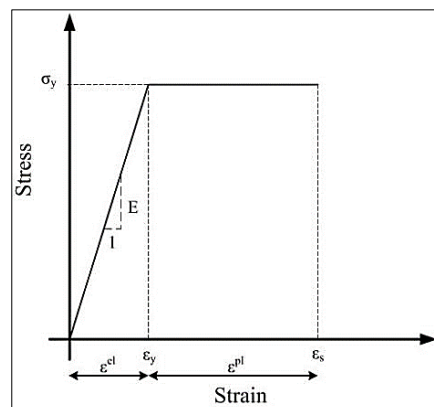


Figure 3. Steel material elastic-plastic material model

$$\varepsilon = \varepsilon^{el} + \varepsilon^{pl} \quad (1)$$

The elastic part is considered to be linear. It can be defined by using Young's Modulus and Poisson's Ratio. While plastic parts can be expressed by using Ultimate Strength. Material properties for continuum Steel pipeline for elastic and plastic behavior can be seen in Table 1.

Table 1. Mechanical properties of steel [35]

Mechanical properties	Term	Value
	Density (kg/m ³)	7850
Elastic property	Young 's modulus (MPa)	210.7 *10 ³
	Poisson 's ratio	0.3
Plastic property	Yield strength (MPa)	490
	Tensile strength (MPa)	690 to 840

• Soil Material

Two types of soil (sandy soil and cohesive soil) were considered to study the interaction between the soil and the buried pipeline. Elastic-plastic analysis was used by Mohr-Coulomb theory as soil mechanical properties. In addition, two types of soil (moist soils and saturated soils) were considered to study the effect of water on soil. Table 2 shows the plastic properties of soils.

Table 2. Mechanical properties of soil [35]

Type of soil	Mechanical properties	Term	Value	
			Moist	Saturated
Sandy soil		Density (kg/m ³)	1850	2160
	Elastic property	Young's modulus (MPa)	24	96
		Poisson's ratio	0.2	0.25
		Cohesive strength (C - kPa)	17	
	Plastic property	Friction angle (ϕ - deg)	40	
		Dilation angle (ψ - deg)	2	
Cohesive soil		Density (kg/m ³)	1700	2000
	Elastic property	Young's modulus (MPa)	19	48
		Poisson's ratio	0.25	0.45
		Cohesive strength (C - kPa)	252	
	Plastic property	Friction angle (ϕ - deg)	29	
		Dilation angle (ψ - deg)	2	

• Concrete Pipeline

The behavior of concrete is characterized as a nonlinear response, which an elastic part can define up to micro-cracking is initiated in the concrete, then the material has nonlinear plastic behavior. CDP model assumes failure to be due to compressive crushing and tensile cracking of the concrete. The two hardening variables $\widetilde{\varepsilon}_c^{pl}$ and $\widetilde{\varepsilon}_t^{pl}$ control the yield surface under compression and tension loading, respectively. The plastic behavior in the compression stage is defined by stress hardening with strain-softening after reaching the ultimate stress σ_{cu} . Equation 2 and 3 [37] shows the characterized of the compressive and tensile stresses:

$$\sigma_c = \sigma_c \left(\widetilde{\varepsilon}_c^{pl}, \widetilde{\varepsilon}_c^{pl}, \theta, f_i \right) \quad (2)$$

$$\sigma_t = \sigma_t \left(\widetilde{\varepsilon}_t^{pl}, \widetilde{\varepsilon}_t^{pl}, \theta, f_i \right) \quad (3)$$

Where, $\widetilde{\varepsilon}_t^{pl}$ and $\widetilde{\varepsilon}_c^{pl}$ are the equivalent plastic strains in tension and compression, respectively; θ is the temperature, $\widetilde{\varepsilon}_c^{pl}$ and $\widetilde{\varepsilon}_t^{pl}$ are the equivalent plastic strain rates, and f_i is any other predefined variables.

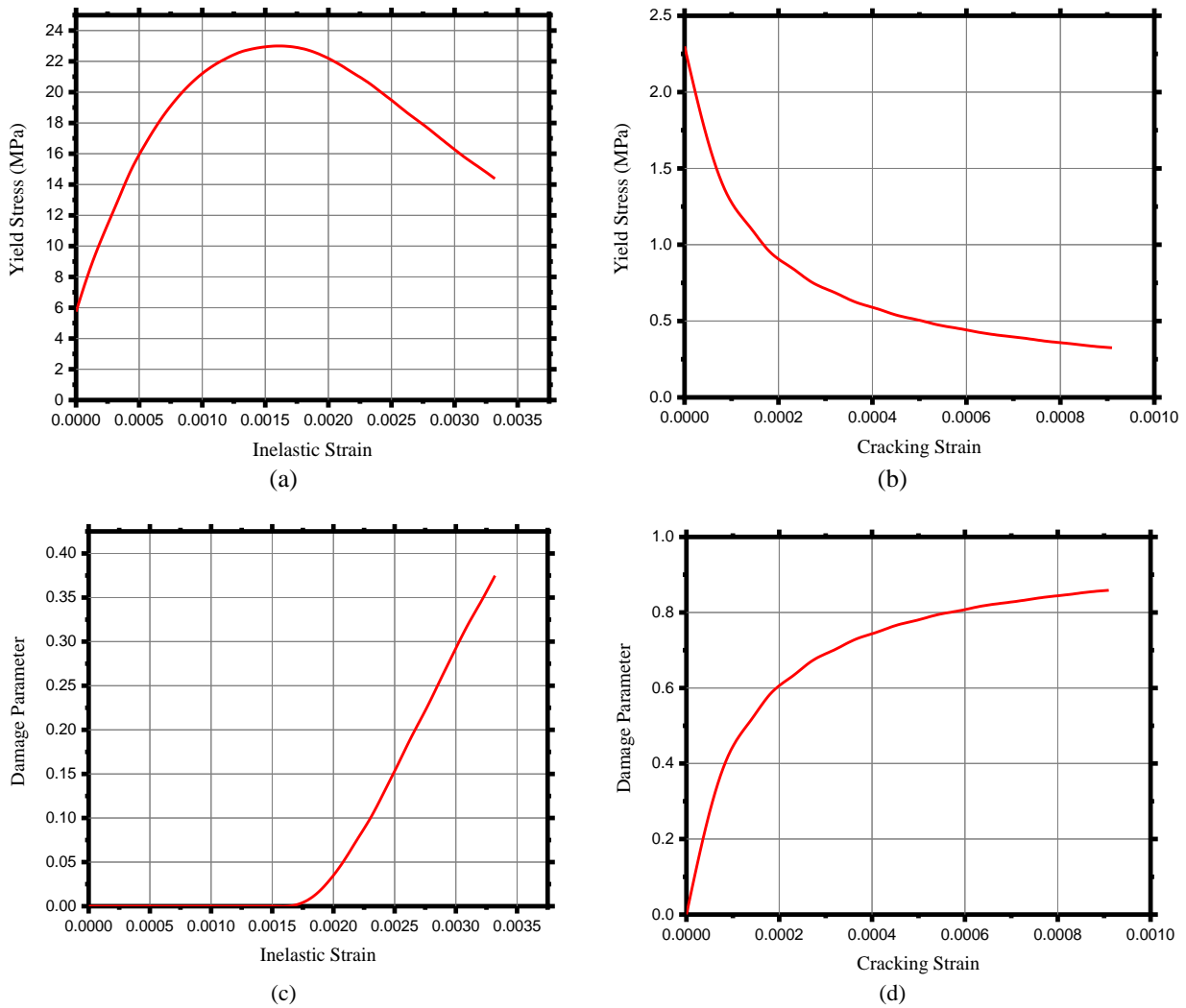


Figure 4. Concrete behavior in (a, c) compression and (b, d) tension

In the ABAQUS software, the CDP model has been used to modify the Drucker-Prager strength hypothesis. In recent years, that model has been modified [38,39]. According to that modification, the failure surface in the deviatoric cross-section needs not to be as circle shape, and parameter K_c determines that. Where parameter K_c is defined as a ratio between the distance of the hydrostatic axis and respectively the tension meridian and the compression meridian in the deviatoric cross-section, that ratio is always bigger than 0.5, and when the value of the ratio equal 1, the deviatoric cross-section of the failure surface becomes as circle shape (as Drucker-Prager strength hypothesis). According to his experimental study, Majewski [40] mentioned that this value for normal stress between [0 to 0.6] slowly increases with decreasing principal stress. The CDP model recommends $K_c=2/3$ [41]. The shape is similar to the strength index (with three mutually tangent ellipses together) [42]. It is a theoretical-experimental index based on tri-axial stress test results, as shown in Figure 5.

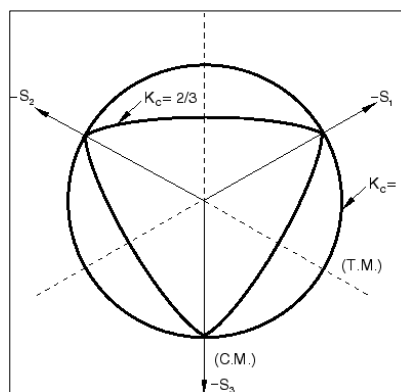


Figure 5. Deviatoric cross-section of failure surface in the CDP model [43]

As well as, the plane's meridians shape in the stress space changes. Experimental studies show that the meridians have curved shapes. In the CDP model, the plastic is characterized by eccentricity (plastic potential eccentricity). A small positive value expresses the rate of approach of the plastic potential hyperbola to its asymptote. Also, it means the length (measured along the hydrostatic axis) of the part located between the intersection of the asymptotes and the vertex of the hyperbola of this hyperbola (the center of the hyperbola). Parameter eccentricity can be characterized as a ratio between tensile strength and compressive strength [44]. The CDP model recommends $\epsilon=0.1$ [41]; When $\epsilon = 0$, the surface in the meridional plane becomes a straight line (as in the case Drucker-Prager hypothesis) [43], as shown in Figure 6.

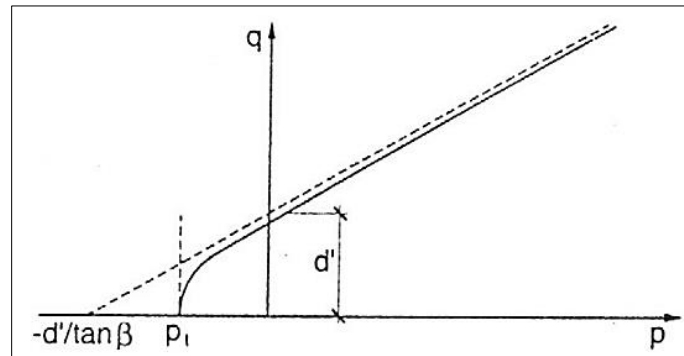


Figure 6. Hyperbolic surface of plastic potential in the meridional plane [43]

Another parameter describing the CDP is the point in which the concrete is under failure under biaxial compression. Figure 7 shows the Concrete Strength under biaxial stress. σ_{b0}/σ_{c0} (f_{b0}/f_{c0}) is a strength ratio in the biaxial case to the strength in the uniaxial case. The ABAQUS user's manual recommends $\sigma_{b0}/\sigma_{c0}=1.16$ [41].

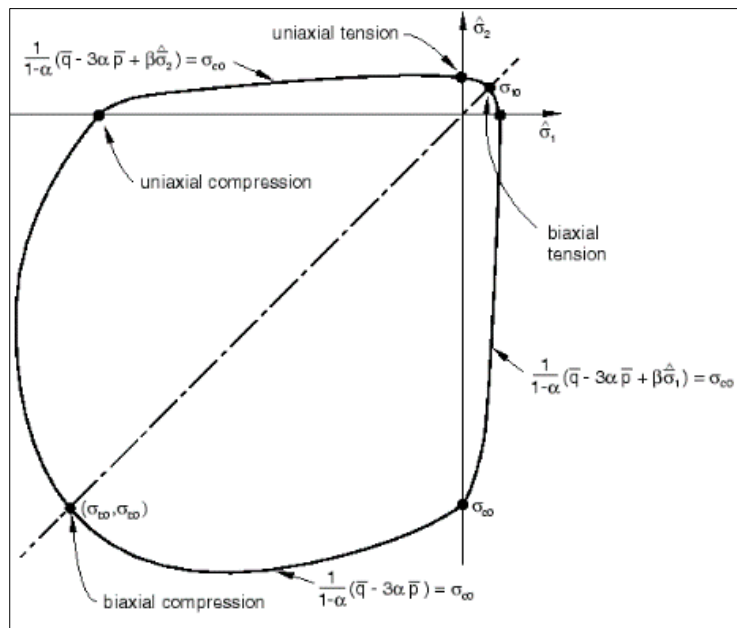


Figure 7. Strength of concrete under biaxial stress in the CDP model [43]

The additional parameter describing the CDP is *dilation angle*, i.e., the angle of the failure surface inclined toward the hydrostatic axis, measured in the meridional plane. Generally, dilation angle ψ is considered as a concrete internal friction angle. The CDP model recommends $\psi= (36^\circ - 40^\circ)$ [43]. The last parameter is the Viscosity parameter, μ , used for the visco-plastic regularisation of the concrete constitutive equations in Abaqus/Standard analyses. This parameter is ignored in Abaqus/Explicit. The default value is 0.0 [41]. Table 3 shows the parameters that characterize the Concrete Damaged Plasticity.

Table 3. Parameters that characterize the Concrete Damaged Plasticity

Parameter name	Dilatation angle	Eccentricity	f_{b0}/f_{c0}	K	Viscosity parameter
Value	36	0.1	1.16	0.667	0

• 3D-printed Concrete Pipeline

According to previous studies, the currently unacceptable constitutive model of 3DPC can be found. Anyway, it is thought that there is no 3DPC anisotropic behavior before filament deposition and adhesion. The 3DPC structures asymmetry is due to the adhesive interface between threads interconnected in vertical and horizontal directions. The material parameters used in this study were entirely related to the 3D-printed concrete obtained by relevant tests, including compressive strength, etc., which could reflect the nonlinear constitutive properties of the concrete materials. In particular, in the study by Xiao et al. [45], similar methods and the damaged concrete plasticity (CDP) model were adopted to simulate the mechanical properties of 3D printed concrete. Currently, intangible concrete mortars, strictly speaking, are mainly used in 3D printing. There is no recognized model of the foundational relationship of concrete mortar at the moment. However, since both mortar and concrete are semi-brittle materials [46]. It is thought that the plastic damage model of concrete can also be used to simulate the mortar mechanical properties. Therefore, the use of the foundational model of concrete to simulate the properties of the mortar will not affect the results of this study.

2.2. Interaction Model

To describe and position the contacts between the above models, the interaction between the pipeline surrounding surface and the soil interior surface is considered as a fully bounding surface, that for three assumptions (in section 2) where the soil and pipeline are perfectly interconnected, and the interaction between the soil and pipeline is interconnected. Soil and pipes are perfect without flaws. In order to define the contacts between the layers of the 3D printed concrete is established as an entirely tied surface [47].

3. Parameter Study

In this study, it was studied many parameters study, as follow:

- The thickness of the pipeline: 20, 30, and 40 mm;
- Soil type: sandy and cohesive soil;
- Material of the pipeline: steel, concrete, and 3D printed concrete pipeline.

Table 4 shows all the parameters studied:

Table 4. Parameters studied

t (mm)	Soil	Materials			
		Steel	Concrete	3DCP	
20	Sandy Soil	Moist	M-S-1	M-C-1	M-3D-1
		Saturated	M-S-2	M-C-2	M-3D-2
	Cohesive Soil	Moist	M-S-3	M-C-3	M-3D-3
		Saturated	M-S-4	M-C-4	M-3D-4
30	Sandy Soil	Moist	M-S-5	M-C-5	M-3D-5
		Saturated	M-S-6	M-C-6	M-3D-6
	Cohesive Soil	Moist	M-S-7	M-C-7	M-3D-7
		Saturated	M-S-8	M-C-8	M-3D-8
40	Sandy Soil	Moist	M-S-9	M-C-9	M-3D-9
		Saturated	M-S-10	M-C-10	M-3D-10
	Cohesive Soil	Moist	M-S-11	M-C-11	M-3D-11
		Saturated	M-S-12	M-C-12	M-3D-12

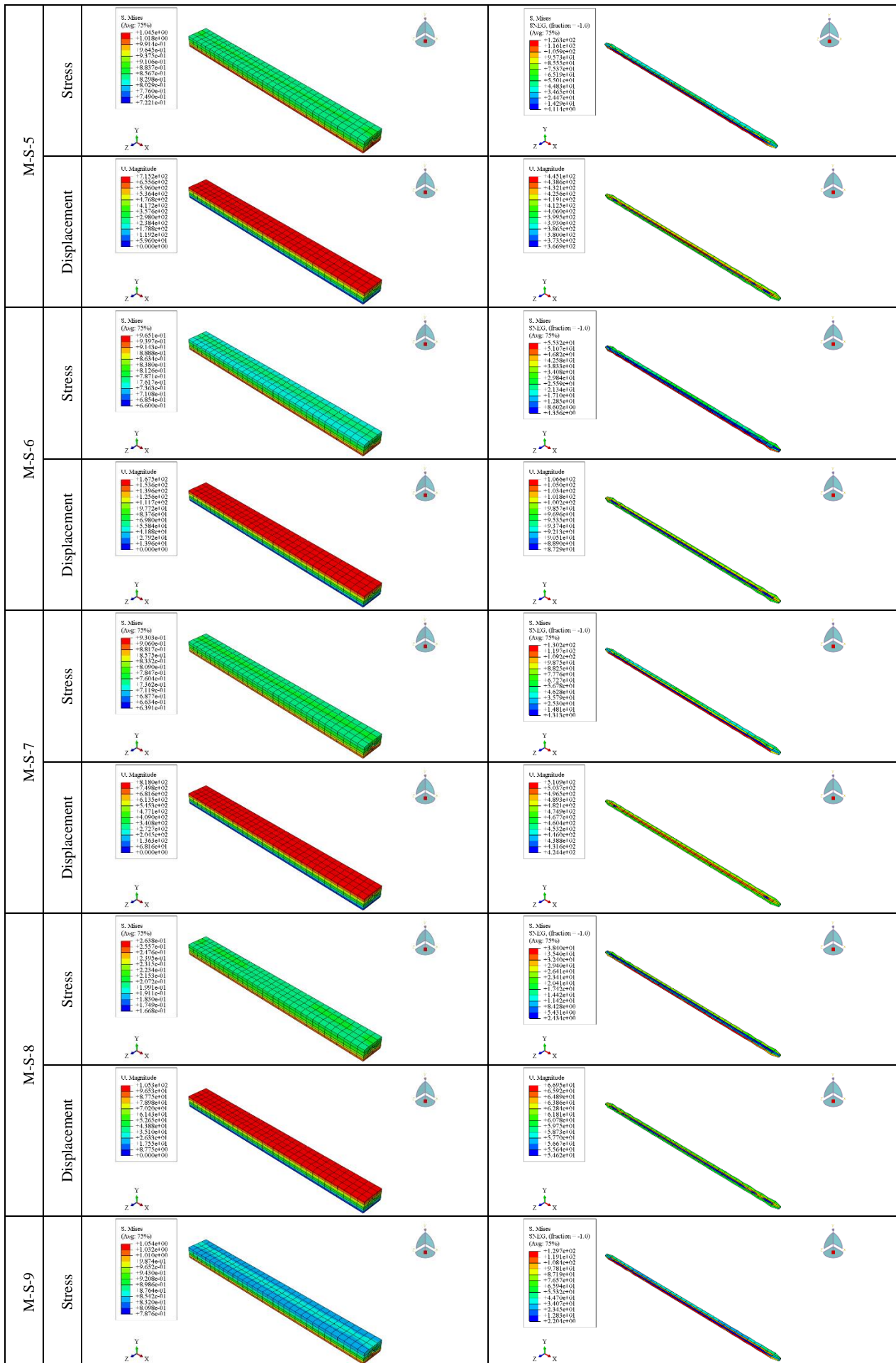
4. Results and Discussion

4.1. Results of the Simulation

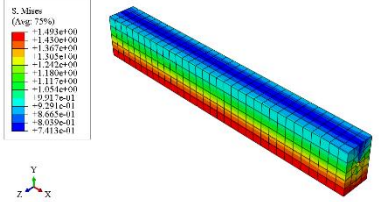
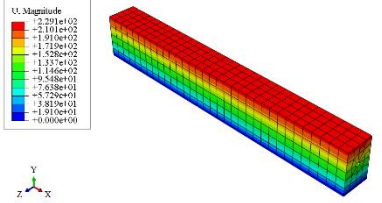
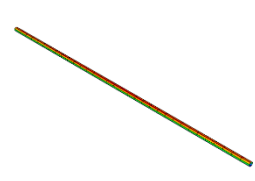
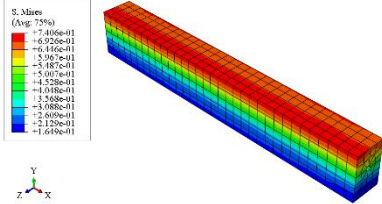
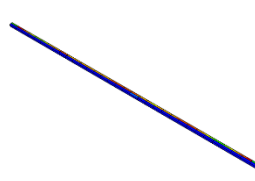
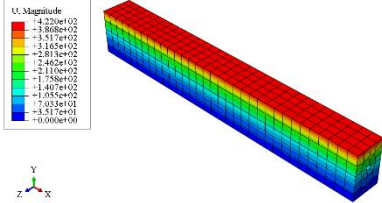
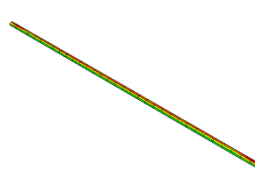
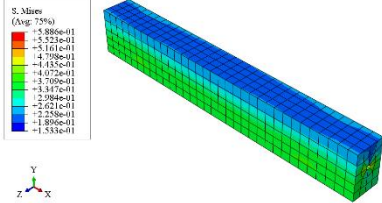
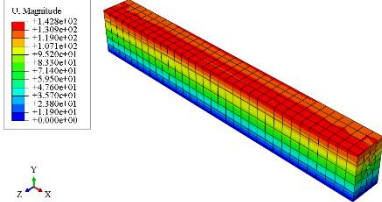
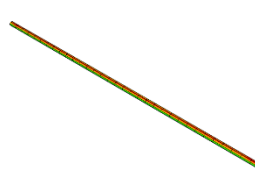
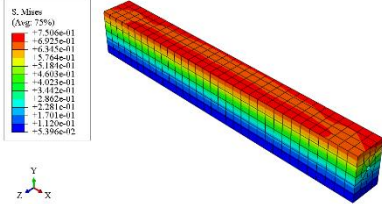
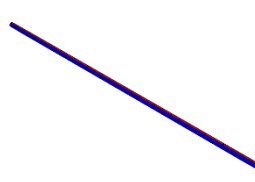
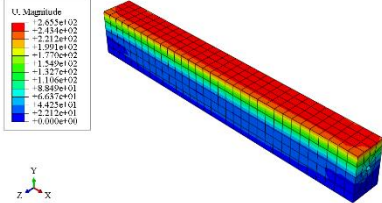
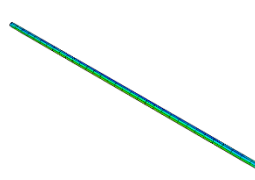
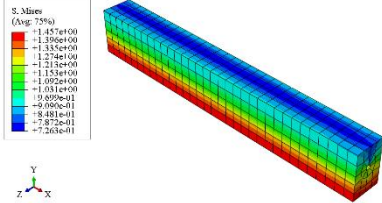
In this study, it was compared between the models by displacement (U, Magnitude; mm) and stress (S, Von Mises; MPa). According to the three basic assumptions mentioned in section 2, many results were obtained. Where these assumptions were affected on the general behavior of the structural. Table 5 shows all the simulation results.

Table 5. All the simulation results

		Soil	Pipeline
M-S-1	Stress		
	Displacement		
M-S-2	Stress		
	Displacement		
M-S-3	Stress		
	Displacement		
M-S-4	Stress		
	Displacement		



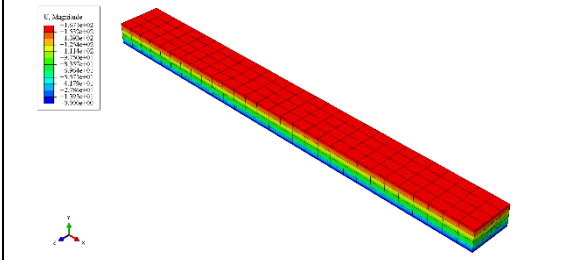
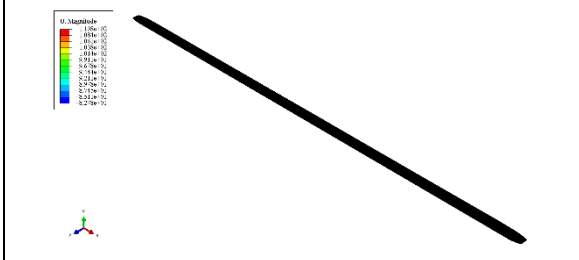
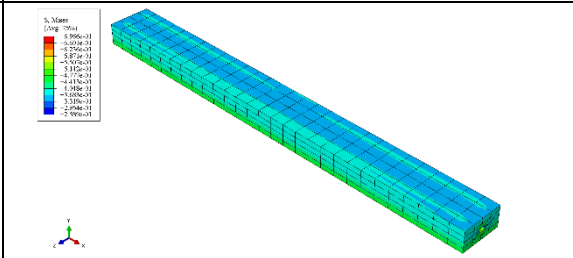
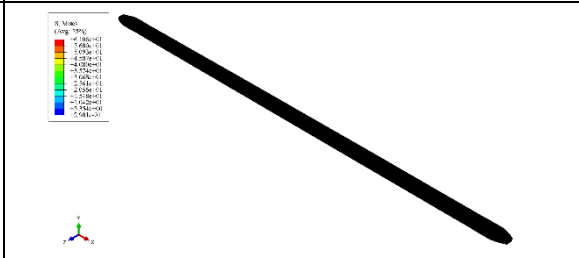
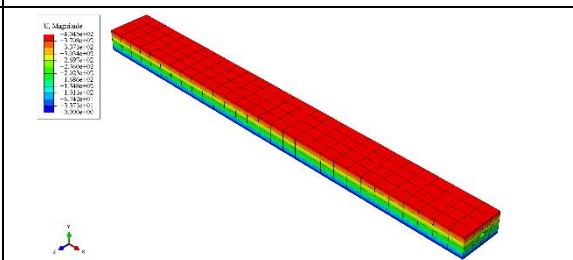
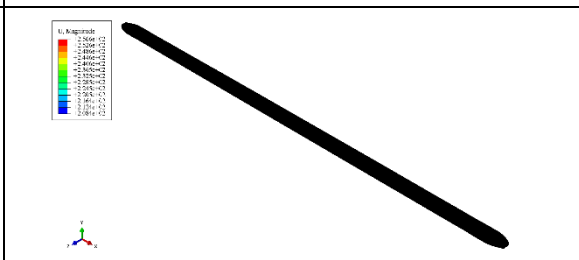
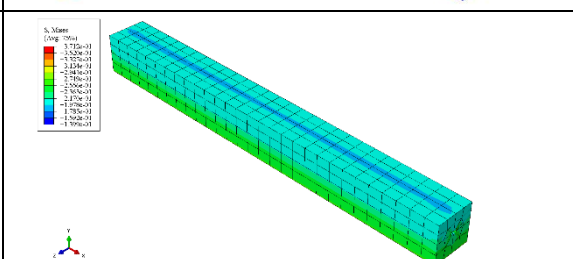
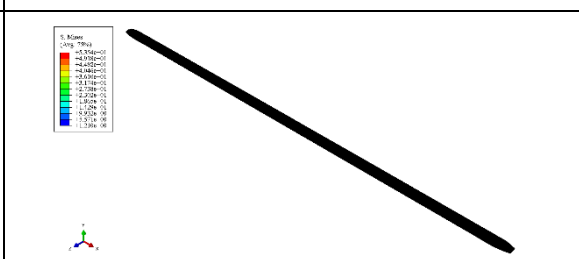
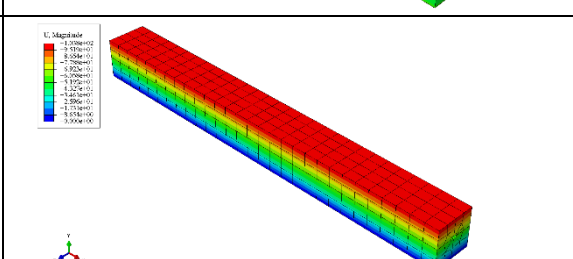
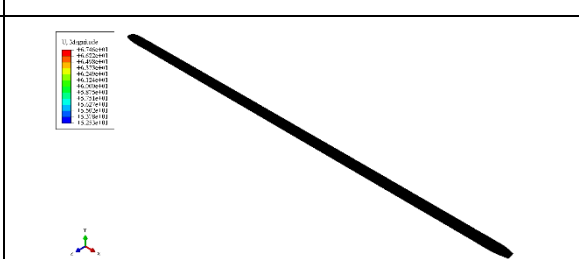
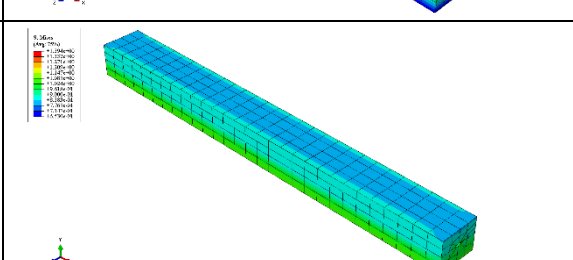
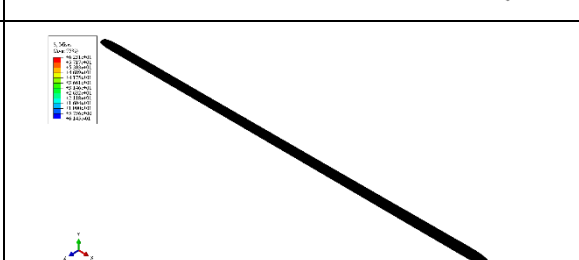
M-S-10	Displacement		
	Stress		
M-S-11	Displacement		
	Stress		
M-S-12	Displacement		
	Stress		
M-C-1	Displacement		
	Stress		

M-C-2	Stress	 <p>S. Mises (Avg. 75%)</p> <ul style="list-style-type: none"> 1.493e+00 1.350e+00 1.367e+00 1.345e+00 -1.242e+00 1.180e+00 -1.117e+00 -1.054e+00 9.917e-01 -9.291e-01 -8.665e-01 -8.039e-01 -7.413e-01 		 <p>S. Mises S.N.G. (fracture -1.0) (Avg. 75%)</p> <ul style="list-style-type: none"> -1.152e+01 -1.108e+01 -1.021e+01 -9.580e+00 -8.907e+00 -8.254e+00 -7.601e+00 -6.948e+00 -6.294e+00 -5.641e+00 -4.988e+00 -4.335e+00 -3.681e+00 	
	Displacement	 <p>U. Magnitude</p> <ul style="list-style-type: none"> 2.201e+02 -2.101e+02 1.910e+02 1.719e+02 1.528e+02 1.337e+02 1.146e+02 9.548e+01 7.638e+01 5.728e+01 3.819e+01 1.909e+01 -0.000e+00 		 <p>U. Magnitude</p> <ul style="list-style-type: none"> 1.842e+02 -1.688e+02 -1.534e+02 -1.380e+02 -1.226e+02 -1.072e+02 -9.184e+01 -7.596e+01 -6.008e+01 -4.420e+01 -2.832e+01 -1.244e+01 -1.236e+02 	
M-C-3	Stress	 <p>S. Mises (Avg. 75%)</p> <ul style="list-style-type: none"> 7.106e+01 -6.926e+01 -6.16e+01 5.967e+01 -5.187e+01 -5.007e+01 4.228e+01 -4.048e+01 3.268e+01 -3.088e+01 -2.609e+01 -2.129e+01 -1.649e+01 		 <p>S. Mises S.N.G. (fracture -1.0) (Avg. 75%)</p> <ul style="list-style-type: none"> -1.643e+01 -1.507e+01 -1.372e+01 -1.236e+01 -1.101e+01 -9.652e+00 -8.303e+00 -6.954e+00 -5.604e+00 -4.255e+00 -2.906e+00 -1.557e+00 -1.652e+01 	
	Displacement	 <p>U. Magnitude</p> <ul style="list-style-type: none"> 4.220e+02 -3.808e+02 -3.397e+02 3.163e+02 -2.913e+02 2.462e+02 -2.110e+02 -1.758e+02 -1.407e+02 -1.055e+02 -7.044e+01 -3.533e+01 -0.000e+00 		 <p>U. Magnitude</p> <ul style="list-style-type: none"> 1.762e+02 -1.690e+02 -1.618e+02 -1.546e+02 -1.474e+02 -1.402e+02 -1.331e+02 -1.259e+02 -1.187e+02 -1.115e+02 -1.044e+02 -9.713e+01 -8.994e+01 	
M-C-4	Stress	 <p>S. Mises (Avg. 75%)</p> <ul style="list-style-type: none"> 5.886e+01 -5.121e+01 -4.798e+01 -4.133e+01 -4.072e+01 3.709e+01 -3.347e+01 2.984e+01 -2.621e+01 -2.258e+01 -1.895e+01 -1.533e+01 		 <p>S. Mises S.N.G. (fracture -1.0) (Avg. 75%)</p> <ul style="list-style-type: none"> -1.542e+01 -1.428e+01 -1.314e+01 -1.200e+01 -1.086e+01 -9.719e+00 -8.581e+00 -7.443e+00 -6.304e+00 -5.166e+00 -4.027e+00 -2.889e+00 -1.751e+00 	
	Displacement	 <p>U. Magnitude</p> <ul style="list-style-type: none"> 1.428e+02 -1.300e+02 -1.190e+02 1.071e+02 -9.520e+01 8.330e+01 -7.140e+01 -5.950e+01 -4.760e+01 -3.570e+01 -2.380e+01 -1.190e+01 -0.000e+00 		 <p>U. Magnitude</p> <ul style="list-style-type: none"> 1.072e+02 -1.025e+02 -9.822e+01 -9.374e+01 -8.926e+01 -8.478e+01 -8.030e+01 -7.582e+01 -7.134e+01 -6.686e+01 -6.238e+01 -5.790e+01 -5.309e+01 	
M-C-5	Stress	 <p>S. Mises (Avg. 75%)</p> <ul style="list-style-type: none"> 7.506e+01 -6.923e+01 -6.345e+01 5.768e+01 -5.184e+01 -4.602e+01 -4.023e+01 -3.442e+01 2.862e+01 -2.281e+01 -1.701e+01 -1.120e+01 -5.386e+02 		 <p>S. Mises S.N.G. (fracture -1.0) (Avg. 75%)</p> <ul style="list-style-type: none"> -1.650e+01 -1.531e+01 -1.418e+01 -1.288e+01 -1.161e+01 -1.034e+01 -9.078e+00 -7.811e+00 -6.545e+00 -5.278e+00 -4.012e+00 -2.746e+00 -1.485e+00 -1.785e+01 	
	Displacement	 <p>U. Magnitude</p> <ul style="list-style-type: none"> 2.655e+02 -2.434e+02 -2.213e+02 1.991e+02 -1.769e+02 1.549e+02 -1.327e+02 -1.106e+02 8.860e+01 -6.637e+01 -4.424e+01 -2.212e+01 -0.000e+00 		 <p>U. Magnitude</p> <ul style="list-style-type: none"> 1.197e+02 -1.131e+02 -1.066e+02 -1.001e+02 -9.355e+01 -8.701e+01 -8.048e+01 -7.394e+01 -6.740e+01 -6.086e+01 -5.432e+01 -4.778e+01 -4.130e+01 	
M-C-6	Stress	 <p>S. Mises (Avg. 75%)</p> <ul style="list-style-type: none"> 1.457e+00 1.396e+00 1.335e+00 1.274e+00 1.213e+00 1.153e+00 1.092e+00 1.031e+00 0.970e+00 -9.09e-01 -8.481e-01 -7.872e-01 -7.263e-01 		 <p>S. Mises S.N.G. (fracture -1.0) (Avg. 75%)</p> <ul style="list-style-type: none"> -1.220e+01 -1.188e+01 -1.164e+01 -1.083e+01 -1.011e+01 -9.583e+00 -9.058e+00 -8.533e+00 -8.008e+00 -7.483e+00 -6.958e+00 -6.433e+00 -5.908e+00 	

M-C-7	Displacement		
	Stress		
M-C-8	Displacement		
	Stress		
M-C-9	Displacement		
	Stress		
M-C-10	Displacement		
	Stress		

M-C-11	Stress		
	Displacement		
M-C-12	Stress		
	Displacement		
M-3D-1	Stress		
	Displacement		
M-3D-2	Stress		
	Displacement		

M-3D-3	Stress		
	Displacement		
M-3D-4	Stress		
	Displacement		
M-3D-5	Stress		
	Displacement		
M-3D-6	Stress		

M-3D-7	Displacement		
	Stress		
M-3D-8	Displacement		
	Stress		
M-3D-9	Displacement		
	Stress		

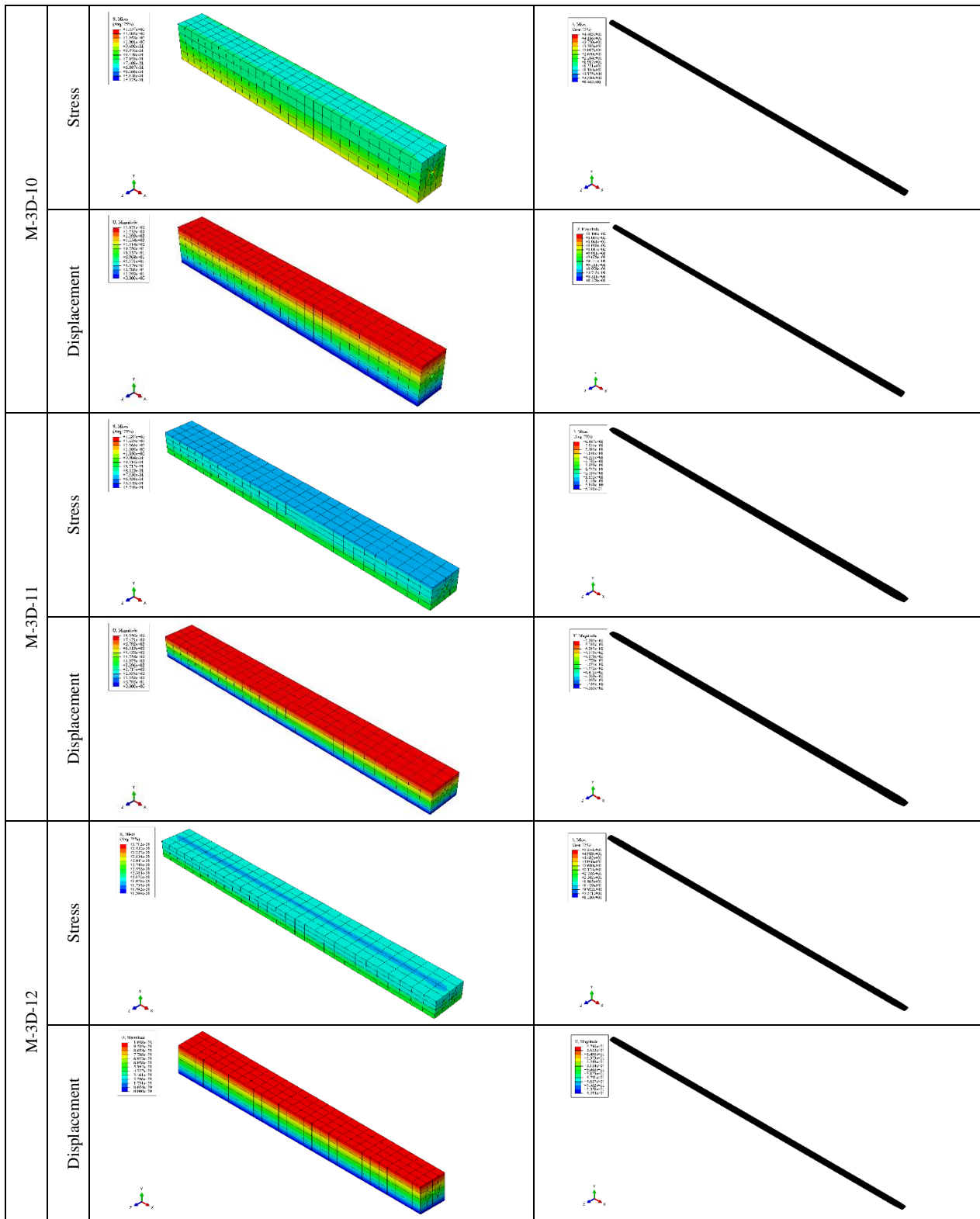


Table 6 shows a summary of all results:

Table 6. Summary of all results

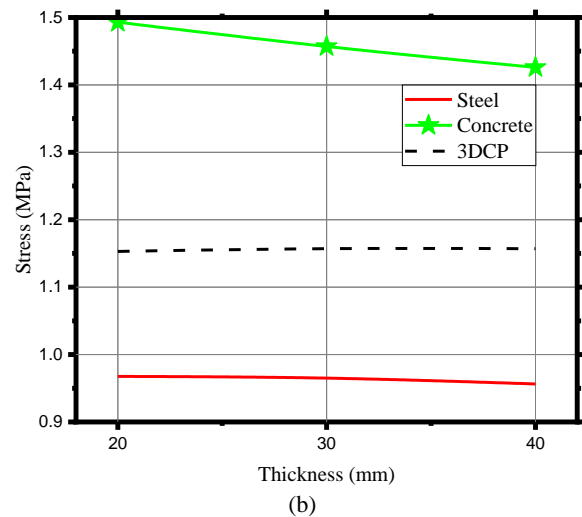
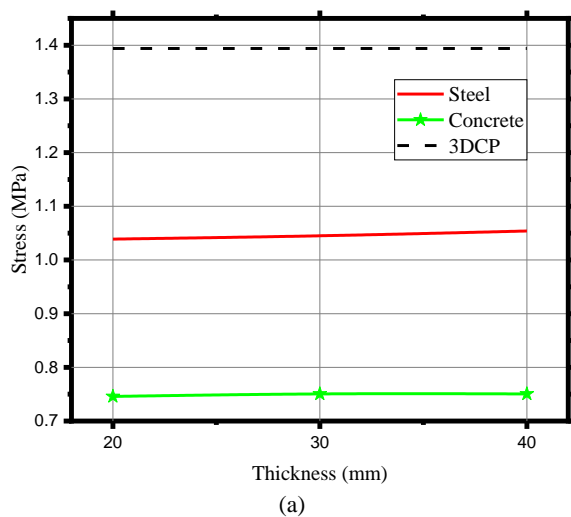
Model	Soil		Pipeline	
	Stress (MPa)	Displacement (mm)	Stress (MPa)	Displacement (mm)
M-S-1	1.039	717.9	119.3	448.9
M-S-2	0.9676	167.8	68.12	107.2
M-S-3	0.9451	8207	125.7	516.2
M-S-4	0.2637	105.7	44.61	67.88
M-S-5	1.045	715.2	126.3	445.1

M-S-6	0.9651	167.5	55.32	106.6
M-S-7	0.9303	818	130.2	510.9
M-S-8	0.2638	105.3	38.4	66.95
M-S-9	1.054	711.5	129.7	440.1
M-S-10	0.9563	167.1	56.9	106.2
M-S-11	0.9344	815.7	132	504.4
M-S-12	0.2595	104.9	33.97	c
M-C-1	0.7459	257.3	16.36	108.4
M-C-2	1.493	229.1	11.52	164.2
M-C-3	0.7406	422	16.43	176.2
M-C-4	0.5886	142.8	15.42	107.2
M-C-5	0.7506	265.5	16.58	119.7
M-C-6	1.457	223.3	12.2	160
M-C-7	0.7672	426.3	16.49	187.6
M-C-8	0.374	120.2	11.22	84.67
M-C-9	0.7506	273.6	16.57	123.2
M-C-10	1.426	217.3	14.49	153.7
M-C-11	0.7973	428.7	16.49	189.2
M-C-12	0.3166	106.3	12.32	72.27
M-3D-1	1.394	712.9	62.31	470.1
M-3D-2	1.153	149.9	45.21	98.54
M-3D-3	1.287	815	64.47	528.5
M-3D-4	0.3712	103.8	53.54	67.46
M-3D-5	1.394	712.9	62.31	470.1
M-3D-6	1.157	167.1	44.83	110.8
M-3D-7	1.287	404.5	61.06	528.5
M-3D-8	0.3712	103.8	53.54	67.46
M-3D-9	1.394	712.9	62.31	470.1
M-3D-10	1.157	167.1	44.83	110.8
M-3D-11	1.287	815	64.47	528.5
M-3D-12	0.3712	103.8	53.54	67.46

5. Discussion of the Simulation

5.1. Soil Stress Results

Figure 8 shows the soil stress results with different thicknesses of the pipeline. The behavior of all types of soil for all pipelines materials was similar behavior in the case of moist soil. As shown from Figure 8 (a), (c), in the case of moist soil, all pipeline materials have similar behaviour with different thicknesses of the pipeline, 3DCP pipeline has higher stress while traditional concrete pipeline has lower stress. On the other hand, in the case of saturated soils, the stress of the traditional concrete pipeline is reduced when the thickness of the pipeline is increased. While 3DCP and Steel pipelines have similar behaviour, as shown in Figure 8 (b), (d). Also, when $t = 30$ mm. Both traditional concrete and 3DCP have the similar pressure. It also was noted that traditional concrete pipes behavior are highly affected due to the presence of cohesive soil saturated



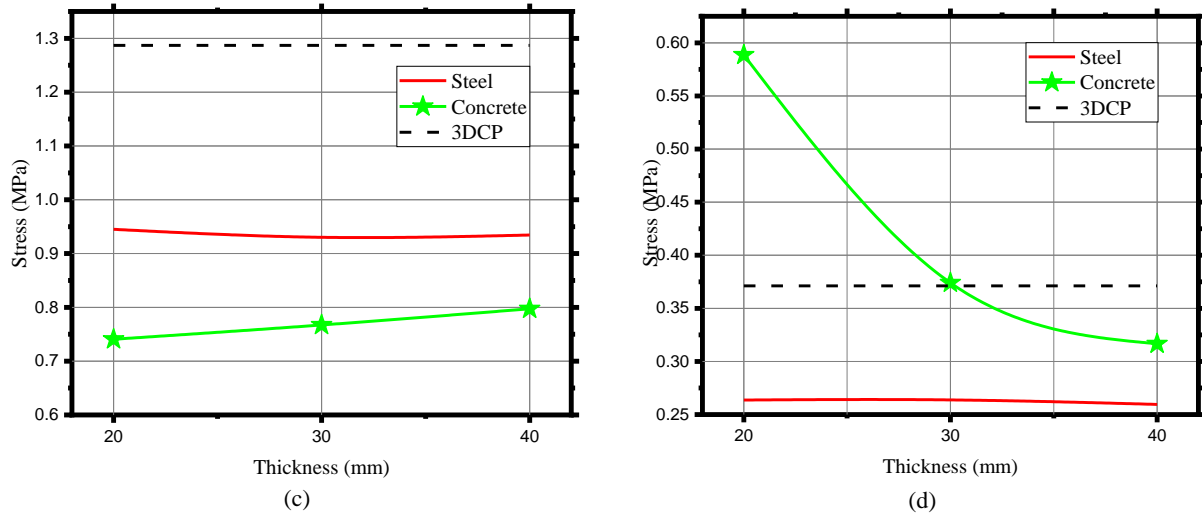


Figure 8. Soil Stress: (a) Sandy soil Moist, (b) Sandy soil Saturated, (c) Cohesive soil Moist, and (d) Cohesive soil Saturated

5.2. Soil Displacement Results

Figure 9 shows the results of soil displacement with different thicknesses of the pipeline. In the case of moist sandy soil Figure 9 (a), all pipeline materials have similar behaviour with different thicknesses of the pipeline. Whereas steel and 3DCP pipelines have the same behaviour, while traditional concrete pipelines have a lower displacement. In the case of saturated sandy soil Figure 9 (b), the displacement of the 3DCP pipeline increases as the thickness of the pipeline increases. While the displacement of the traditional pipeline is reduced when the thickness of the pipeline is increased.

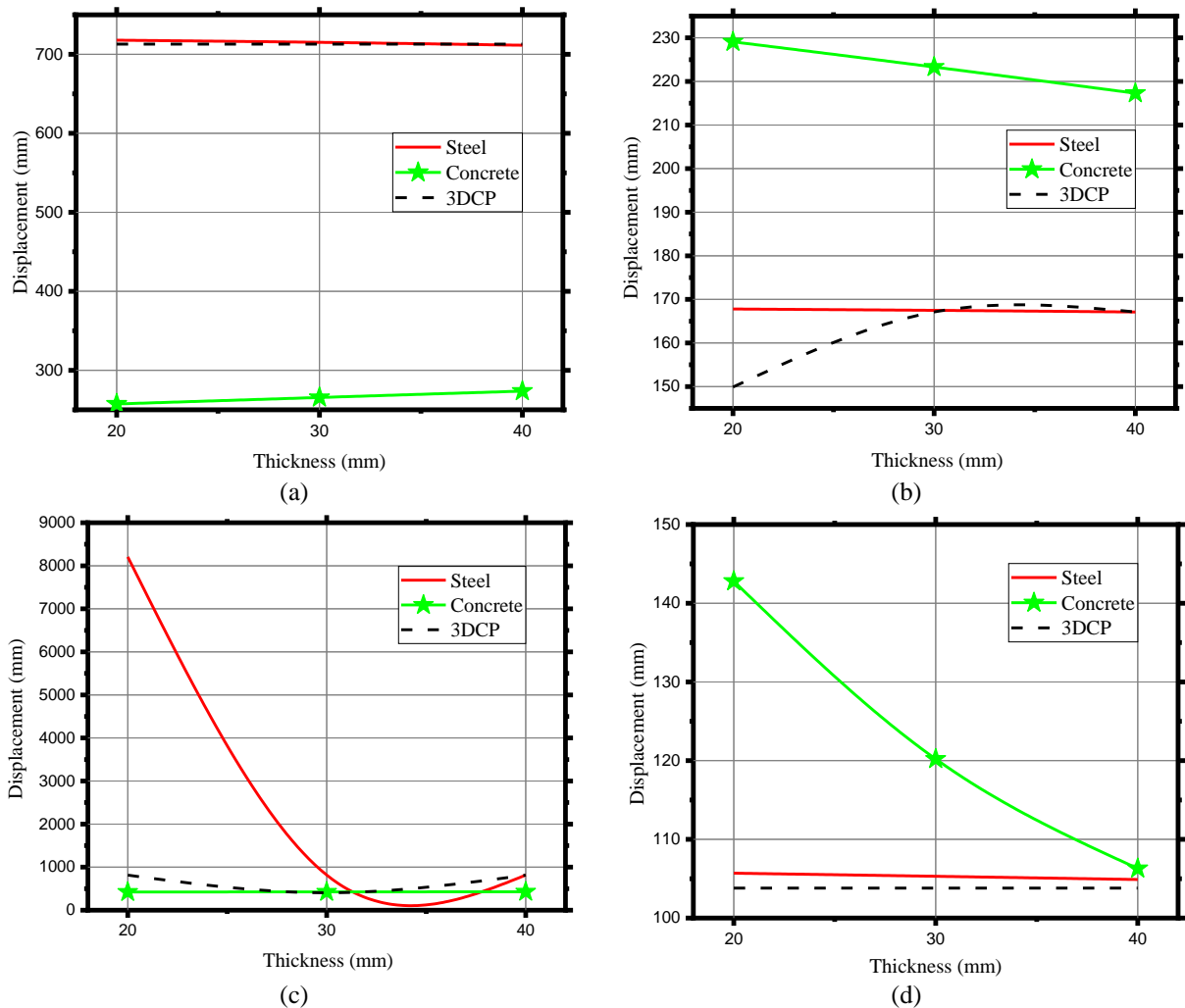


Figure 9. Soil Displacement: (a) Sandy soil Moist, (b) Sandy soil Saturated, (c) Cohesive soil Moist, and (d) Cohesive soil Saturated

In the case of moist cohesive soil Figure 9 (c), the displacement of the steel pipeline is significantly reduced when the thickness of the pipeline is increased, while both traditional concrete pipes and 3DCP pipelines have the same displacement. In the case of saturated cohesive soil Figure 9 (d), the displacement of the traditional concrete pipeline is significantly reduced when the thickness of the pipeline is increased, while the steel and 3DCP pipes have the similar displacement. It also was noted that steel and traditional concrete pipes behavior are highly affected due to the presence of cohesive soil moist and cohesive soil saturated, respectively.

5.3. Pipeline Stress Results

Figure 10 shows the results of pipeline stress with different thicknesses of the pipeline. The behavior of all pipelines materials was similar behavior in the case of moist soil. In the case of moist soil Figure 10 (a), (c), all pipeline materials have the same behaviour with different thicknesses of the pipeline. Where the steel pipeline has higher stress while the traditional concrete pipeline has lower pressure. Similar behaviour was seen in the case of saturated sandy soil Figure 10 (b). While in the case of saturated cohesive soil Figure 10 (d), the 3DCP pipeline has higher stress, on the other hand, the traditional concrete pipeline has lower pressure.

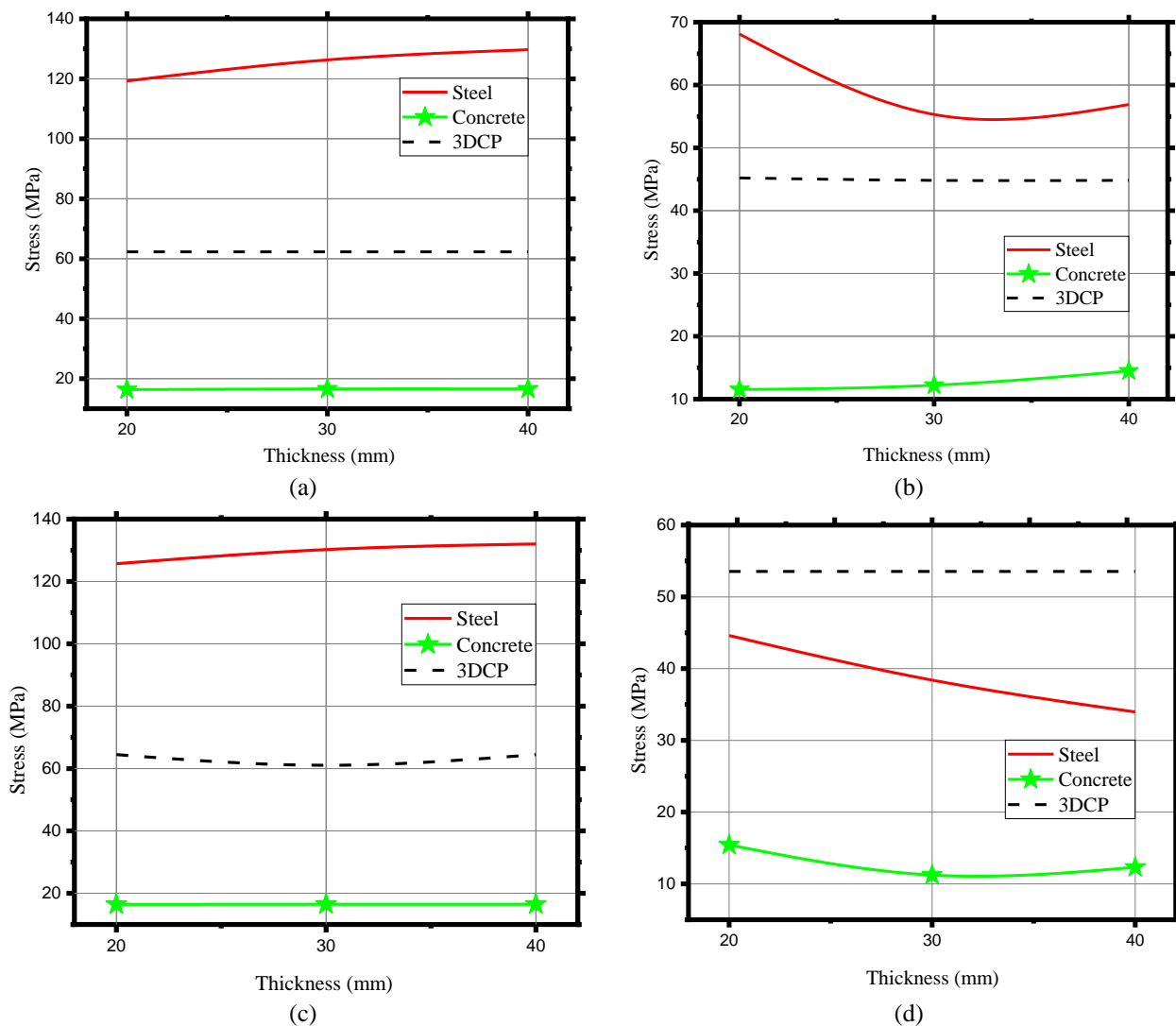


Figure 10 Pipeline Stress: (a) Sandy soil Moist, (b) Sandy soil Saturated, (c) Cohesive soil Moist, and (d) Cohesive soil Saturated

5.4. Pipeline Displacement Results

Figure 11 shows the results of pipeline displacement with different thicknesses of the pipeline. The behavior of all pipelines materials was similar behavior in the case of moist soil .In the case of moist soil Figure 11 (a), (c), all pipeline materials have the same behaviour with different thicknesses of the pipeline. Where both the steel and 3DCP pipelines have higher displacement, while the traditional concrete pipeline has lower displacement. In the case of saturated sandy soil Figure 11 (b), the traditional concrete pipeline has higher displacement. While both steel and 3DCP pipelines have lower displacement. In the case of saturated cohesive soil Figure 11 (d), the displacement of the

traditional concrete pipeline is significantly reduced when the thickness of the pipeline is increased. On the other hand, both steel and 3DCP pipelines have the same displacements. It also was noted that traditional concrete pipes behavior are highly affected due to the presence of cohesive soil saturated.

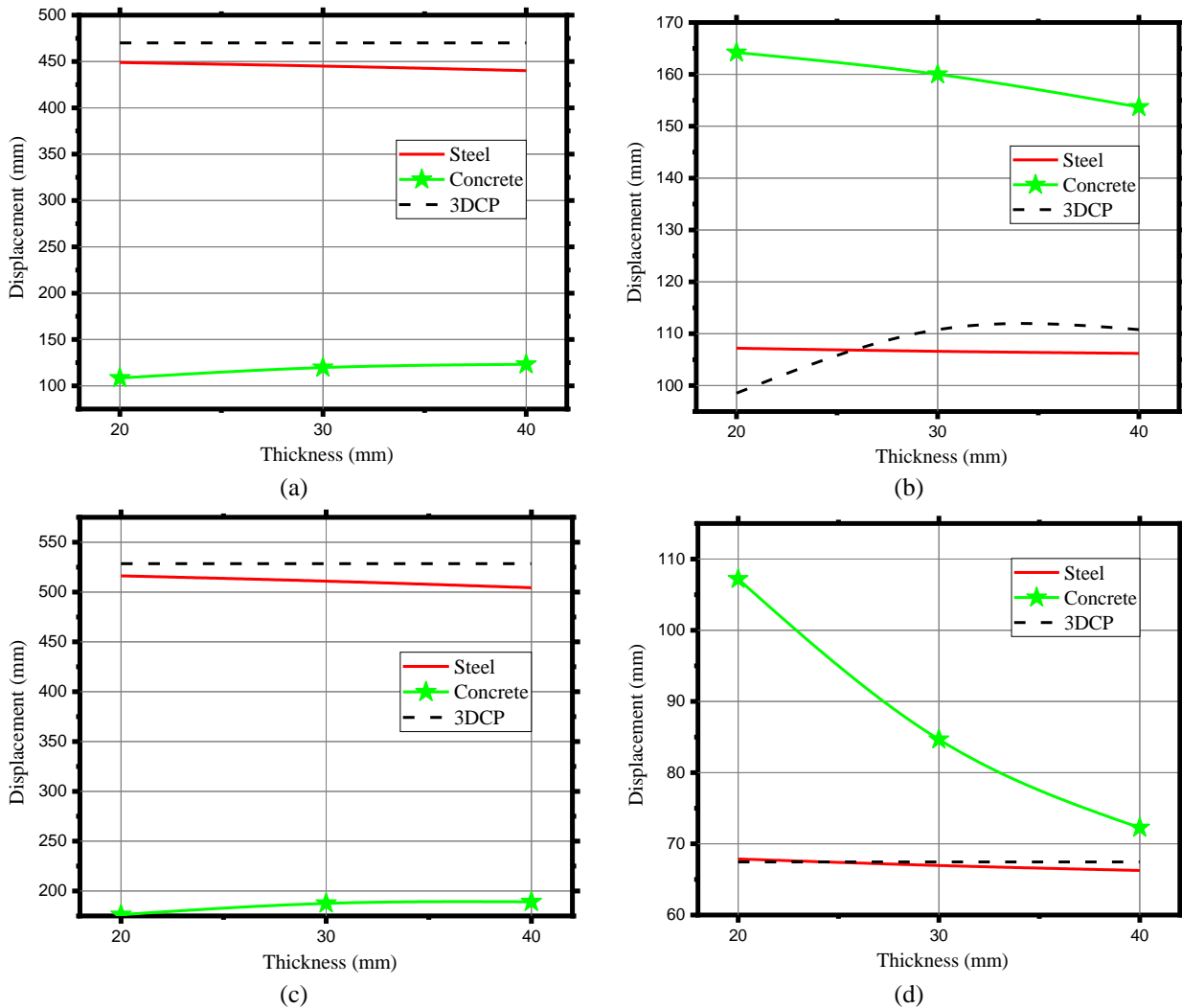


Figure 11. Pipeline Displacement: (a) Sandy soil Moist, (b) Sandy soil Saturated, (c) Cohesive soil Moist, and (d) Cohesive soil Saturated

6. Conclusions

Several parameters were studied in this research as ABAQUS 2020 was used to study the performance of pipelines under static loads. The Von-Mises stress and displacement were used to compare the results. According to the three basic assumptions mentioned in section 2, many results were obtained. Where these assumptions were affected on the general behavior of the structural

- In the case of moist soil, all pipeline materials have similar behavior with different thicknesses. 3DCP pipeline has higher stress while traditional concrete pipeline has lower stress. On the other hand, in the case of saturated soils, the stress of the traditional concrete pipeline is reduced when the thickness of the pipeline is increased. While 3DCP and steel pipelines have similar behavior. Also, when $t = 30$ mm. Both traditional concrete and 3DCP have similar stress.
- In the case of moist sandy soil, all pipeline materials have similar behavior with different thicknesses of the pipeline. At the same time, steel and 3DCP pipelines have the same behavior, while traditional concrete pipelines have a lower displacement. In the case of saturated sandy soil, the displacement of the 3DCP pipeline increases as the thickness of the pipeline increases. At the same time, the displacement of the traditional pipeline is reduced when the thickness of the pipeline is increased. In the case of moist cohesive soil, the displacement of the steel pipeline is significantly reduced when the thickness of the pipeline is increased. At the same time, both traditional concrete pipes and 3DCP pipelines have the same displacement. When $t \geq 30$ mm, all pipeline materials have the same displacement. In the case of saturated cohesive soil, the displacement of the traditional concrete pipeline is

significantly reduced when the thickness of the pipeline is increased. At the same time, the steel and 3DCP pipes have a similar displacement.

- In the case of moist soil, all pipeline materials have the same behavior with different thicknesses of the pipeline. Where the steel pipeline has higher stress while the traditional concrete pipeline has lower pressure. Similar behavior was seen in the case of saturated sandy soil. While in the case of saturated cohesive soil, the 3DCP pipeline has higher stress, on the other hand, the traditional concrete pipeline has lower pressure.
- In the case of moist soil, all pipeline materials have the same behavior with different thicknesses of the pipeline. Both the steel and 3DCP pipelines have higher displacement, while the traditional concrete pipeline has lower displacement. In the case of saturated sandy soil, the traditional concrete pipeline has higher displacement. In contrast, both steel and 3DCP pipelines have lower displacement. In the case of saturated cohesive soil, the displacement of the traditional concrete pipeline is significantly reduced when the thickness of the pipeline is increased. On the other hand, both steel and 3DCP pipelines have the same displacements.
- Different results were obtained depending on the type of soil. The lowest stress of soil was reported in the case of saturated cohesive soil (steel pipeline). In contrast, the lowest stress of pipeline was reported in the case of saturated sandy soil (traditional concrete pipeline). On the other hand, the highest stress of soil was reported in the case of saturated sandy soil (traditional concrete pipeline). In contrast, the highest stress of pipeline was reported in the case of moist sandy soil and moist cohesive soil (steel pipeline).
- The lowest displacement of soil was reported in the case of saturated cohesive soil (3DCP pipeline). In contrast, the lowest displacement of the pipeline was reported in the case of saturated cohesive soil (steel and 3DCP pipeline). on the other hand, the highest displacement of soil was reported in the case of moist cohesive soil (steel pipeline), while the highest displacement of the pipeline was reported in the case of moist cohesive soil (3DCP pipeline)

7. Declarations

7.1. Author Contributions

Conceptualization, M.J.A. and Y.Q.; methodology, K.A.B.; validation, M.J.A., Y.Q. and K.A.B.; formal analysis, K.A.B.; investigation, K.A.B.; resources, Y.Q.; data curation, K.A.B.; writing—original draft preparation, M.J.A.; writing—review and editing, M.J.A.; visualization, K.A.B.; supervision, Y.Q.; project administration, Y.Q.; funding acquisition, Y.Q. All authors have read and agreed to the published version of the manuscript.

7.2. Data Availability Statement

The data presented in this study are available on request from the corresponding author.

7.3. Funding

The authors received no financial support for the research, authorship, and/or publication of this article.

7.4. Conflicts of Interest

The authors declare no conflict of interest.

8. References

- [1] Bulson, P. S., & Saunders, H. (1987). Buried Structures—Static and Dynamic Strength. *Journal of Vibration and Acoustics*, 109(3), 320–321. doi:10.1115/1.3269439.
- [2] Donmez, D., Gencoglu, M., & Donmez, A. A. (2019). Experimental assessment of TRC cylindrical tube-shaped units. *ISEC 2019 - 10th International Structural Engineering and Construction Conference*, 2–7. doi:10.14455/isec.res.2019.74.
- [3] Viparelli, R., De Luca, A., Santorelli, S., & Pizza, A. G. (2001). Pre-stressed concrete large-diameter pipes: joint behaviour during earthquakes. *WIT Transactions on The Built Environment*, 57.
- [4] Wang, S., Liu, F., & Yu, W. (2011). Investigation on computational method for crack of reinforced concrete pipeline under internal pressure retrofitted with FRP. *AEEngineering Plasticity and Its Applications - Proceedings of the 10th Asia-Pacific Conference, AEPAC 2010*, 19–24. doi:10.1142/9789814324052_0004.
- [5] Tahamouli Roudsari, M., Samet, S., Nuraie, N., & Sohaei, S. (2017). Numerically based analysis of buried GRP pipelines under earthquake wave propagation and landslide effects. *Periodica Polytechnica Civil Engineering*, 61(2), 292–299. doi:10.3311/PPci.9339.
- [6] Ozdemir, Z., Coulier, P., Lak, M. A., François, S., Lombaert, G., & Degrande, G. (2013). Numerical evaluation of the dynamic response of pipelines to vibrations induced by the operation of a pavement breaker. *Soil Dynamics and Earthquake Engineering*, 44, 153–167. doi:10.1016/j.soildyn.2012.09.012.

- [7] Ozdemir, Z., Lak, M. A., François, S., Coulier, P., Lombaert, G., & Degrande, G. (2011). A numerical model for the prediction of the response of pipelines due to vibrations induced by the operation of a pavement breaker. *Proceedings of the 8th International Conference on Structural Dynamics, EUROODYN 2011*, July, 928–935.
- [8] Trautmann, C. H., & O'Rourke, T. D. (1985). Lateral force-displacement response of buried pipe. *Journal of Geotechnical Engineering*, 111(9), 1077-1092. doi:10.1061/(ASCE)0733-9410(1985)111:9(1077).
- [9] Trautmann, C. H., O'Rourke, T. D., & Kulhawy, F. H. (1985). Uplift force-displacement response of buried pipe. *Journal of Geotechnical Engineering*, 111(9), 1061-1076. doi: 10.1061/(ASCE)0733-9410(1985)111:9(1061).
- [10] Sakanoue, T., & Yoshizaki, K. (2003). Experimental study on the effect of light-weight backfill for enhancement of earthquake resistance of buried pipelines. *Proceedings of the International Conference on Offshore Mechanics and Arctic Engineering - OMAE*, 2, 699–703. doi:10.1115/OMAE2003-37228.
- [11] Gibson, I., Rosen, D., & Stucker, B. (2015). *Additive Manufacturing Technologies*. doi:10.1007/978-1-4939-2113-3.
- [12] Huang, S. H., Liu, P., Mokasdar, A., & Hou, L. (2013). Additive manufacturing and its societal impact: A literature review. *International Journal of Advanced Manufacturing Technology*, 67(5–8), 1191–1203. doi:10.1007/s00170-012-4558-5.
- [13] Vaezi, M., Seitz, H., & Yang, S. (2013). A review on 3D micro-additive manufacturing technologies. *International Journal of Advanced Manufacturing Technology*, 67(5–8), 1721–1754. doi:10.1007/s00170-012-4605-2.
- [14] Chua, C. K., Wong, C. H., & Yeong, W. Y. (2017). *Standards, quality control, and measurement sciences in 3D printing and additive manufacturing*. Academic Press.
- [15] Maas, G., & Van Gassel, F. (2005). The influence of automation and robotics on the performance construction. *Automation in Construction*, 14(4), 435–441. doi:10.1016/j.autcon.2004.09.010.
- [16] Zavadskas, E. K. (2010). Automation and robotics in construction: International research and achievements. *Automation in Construction*, 19(3), 286–290. doi:10.1016/j.autcon.2009.12.011.
- [17] Kittusamy, N. K., & Buchholz, B. (2004). Whole-body vibration and postural stress among operators of construction equipment: A literature review. *Journal of Safety Research*, 35(3), 255–261. doi:10.1016/j.jsr.2004.03.014.
- [18] Meliá, J. L., Mearns, K., Silva, S. A., & Lima, M. L. (2008). Safety climate responses and the perceived risk of accidents in the construction industry. *Safety Science*, 46(6), 949–958. doi:10.1016/j.ssci.2007.11.004.
- [19] OSHD Annual Report (2017) - Ministry of Manpower, Occupational Safety And Health Division; Singapore.
- [20] Azhar, S. (2011). Building information modeling (BIM): Trends, benefits, risks, and challenges for the AEC industry. *Leadership and Management in Engineering*, 11(3), 241–252. doi:10.1061/(ASCE)LM.1943-5630.0000127.
- [21] Bryde, D., Broquetas, M., & Volm, J. M. (2013). The project benefits of building information modelling (BIM). *International Journal of Project Management*, 31(7), 971–980. doi:10.1016/j.ijproman.2012.12.001.
- [22] Conner, B. P., Manogharan, G. P., Martof, A. N., Rodomsky, L. M., Rodomsky, C. M., Jordan, D. C., & Limperos, J. W. (2014). Making sense of 3-D printing: Creating a map of additive manufacturing products and services. *Additive Manufacturing*, 1, 64–76. doi:10.1016/j.addma.2014.08.005.
- [23] Thomas, D. S., & Gilbert, S. W. (2014). Costs and cost effectiveness of additive manufacturing. *NIST special publication*, 1176, 12. doi:10.6028/nist.sp.1176.
- [24] Kothman, I., & Faber, N. (2016). How 3D printing technology changes the rules of the game Insights from the construction sector. *Journal of Manufacturing Technology Management*, 27(7), 932–943. doi:10.1108/JMTM-01-2016-0010.
- [25] Newman, J., & Choo, B. S. (2003). Advanced concrete technology. In *Advanced Concrete Technology*. Elsevier. doi:10.1016/B978-0-7506-5686-3.X5246-X.
- [26] Souza, M. T., Ferreira, I. M., Guzi de Moraes, E., Senff, L., & Novaes de Oliveira, A. P. (2020). 3D printed concrete for large-scale buildings: An overview of rheology, printing parameters, chemical admixtures, reinforcements, and economic and environmental prospects. *Journal of Building Engineering*, 32(September). doi:10.1016/j.jobe.2020.101833.
- [27] Kristombu Baduge, S., Navaratnam, S., Abu-Zidan, Y., McCormack, T., Nguyen, K., Mendis, P., Zhang, G., & Aye, L. (2021). Improving performance of additive manufactured (3D printed) concrete: A review on material mix design, processing, interlayer bonding, and reinforcing methods. *Structures*, 29(November), 1597–1609. doi:10.1016/j.istruc.2020.12.061.
- [28] Hambach, M., & Volkmer, D. (2017). Properties of 3D-printed fiber-reinforced Portland cement paste. *Cement and Concrete Composites*, 79, 62–70. doi:10.1016/j.cemconcomp.2017.02.001.
- [29] Marchment, T., & Sanjayan, J. (2020). Mesh reinforcing method for 3D Concrete Printing. *Automation in Construction*, 109(102992). doi:10.1016/j.autcon.2019.102992.

- [30] Clare Scott. (2016). Chinese Construction Company 3D Prints an Entire Two-Story House On-Site in 45 Days | 3DPrint.com | The Voice of 3D Printing / Additive Manufacturing. 16.07.2016, 1–5. Available online: <https://3dprint.com/138664/huashang-tengda-3d-print-house/> (accessed on May 2021).
- [31] Le, T. T., Austin, S. A., Lim, S., Buswell, R. A., Gibb, A. G. F., & Thorpe, T. (2012). Mix design and fresh properties for high-performance printing concrete. *Materials and Structures*, 45(8), 1221–1232. doi:10.1617/s11527-012-9828-z.
- [32] Le, T. T., Austin, S. A., Lim, S., Buswell, R. A., Law, R., Gibb, A. G. F., & Thorpe, T. (2012). Hardened properties of high-performance printing concrete. *Cement and Concrete Research*, 42(3), 558–566. doi:10.1016/j.cemconres.2011.12.003.
- [33] Salet, T. A. M., Ahmed, Z. Y., Bos, F. P., & Laagland, H. L. M. (2018). Design of a 3D printed concrete bridge by testing*. *Virtual and Physical Prototyping*, 13(3), 222–236. doi:10.1080/17452759.2018.1476064.
- [34] Asprone, D., Menna, C., Bos, F. P., Salet, T. A. M., Mata-Falcón, J., & Kaufmann, W. (2018). Rethinking reinforcement for digital fabrication with concrete. *Cement and Concrete Research*, 112, 111–121. doi:10.1016/j.cemconres.2018.05.020.
- [35] Lee, H. (2010). Finite element analysis of a buried pipeline 2010. In University of Manchester (pp. 18–25).
- [36] EN 10224:2002/A1:2005. (2005), Nonalloy steel tubes and fittings for conveying water and other aqueous liquid - Technical delivery conditions, Technical.
- [37] Carreira, D. J., & Chu, K. H. (1985). Stress-Strain Relationship for Plain Concrete in Compression. *Journal of the American Concrete Institute*, 82(6), 797–804. doi:10.14359/10390.
- [38] Lubliner, J., Oliver, J., Oller, S., & Oñate, E. (1989). A plastic-damage model for concrete. *International Journal of Solids and Structures*, 25(3), 299–326. doi:10.1016/0020-7683(89)90050-4.
- [39] Lee, J., & Fenves, G. L. (1998). Plastic-Damage Model for Cyclic Loading of Concrete Structures. *Journal of Engineering Mechanics*, 124(8), 892–900. doi:10.1061/(asce)0733-9399(1998)124:8(892).
- [40] Majewski, S. (2003). The mechanics of structural concrete in terms of elasto-plasticity. Publishing House of Silesian University of Technology, Gliwice.
- [41] Abaqus, G. (2011). Abaqus 6.11. Dassault Systemes Simulia Corporation, Providence, RI, USA.
- [42] Willam, K. J., & Warnke, E. P. (1975). Constitutive model for the triaxial behavior of concrete international association for bridge and structure engineering. In In: Proc. int. association for bridge and structural eng. (pp. 1–30).
- [43] Kmiecik, P., & Kamiński, M. (2011). Modelling of reinforced concrete structures and composite structures with concrete strength degradation taken into consideration. *Archives of Civil and Mechanical Engineering*, 11(3), 623–636. doi:10.1016/s1644-9665(12)60105-8.
- [44] Jankowiak, I., Kakol, W., & Madaj, A. (2005). Identification of numerical model of the continuous composite beam based on experimental tests. In Proceedings of 7th International Conference on Composite Structures, Zielona Góra, Poland, 163-178.
- [45] Xiao, J., Liu, H., & Ding, T. (2021). Finite element analysis on the anisotropic behavior of 3D printed concrete under compression and flexure. *Additive Manufacturing*, 39, 101712. doi:10.1016/j.addma.2020.101712.
- [46] Chang, X., Wang, G., Tang, C., & Ru, Z. (2015). Dynamic behavior of cement-mortar cavern reinforced by bars. *Engineering Failure Analysis*, 55, 343–354. doi:10.1016/j.engfailanal.2015.07.020.
- [47] Ooms, T., Vantghem, G., Van Coile, R., & De Corte, W. (2021). A parametric modelling strategy for the numerical simulation of 3D concrete printing with complex geometries. *Additive Manufacturing*, 38, 101743. doi:10.1016/j.addma.2020.101743.